

Self-assembled titania–silica–sepiolite based nanocomposites for water decontamination†

Marina Nieto-Suárez,^a Giovanni Palmisano,^{b,c} María Luisa Ferrer,^{*a} María Concepción Gutiérrez,^a Sedat Yurdakal,^{b,d} Vincenzo Augugliaro,^{*b} Mario Pagliaro^c and Francisco del Monte^a

Received 8th August 2008, Accepted 19th December 2008

First published as an Advance Article on the web 11th February 2009

DOI: 10.1039/b813864h

This work describes the preparation of microchannel structured monolithic pieces by the “ice-segregation induced self-assembly” (ISISA) process. The monoliths exhibit a hierarchical structure composed of homogeneously mixed colloidal silica resulting from hydrolysis and condensation of an alkoxy silane precursor (*e.g.*, TEOS) and TiO₂ polycrystalline nanoparticles adsorbed onto sepiolite fibres. The combination of such a different species into a single macroporous structure provides a multifunctional material capable of water decontamination by pollutant removal from aqueous media (*via* adsorption on sepiolite) and subsequent elimination by UV irradiation (*via* photocatalytic oxidation on TiO₂ nanoparticles). The performance of the resulting materials has been studied using two organic compounds often present in wastewater such as *p*-nitrophenol (PNP) and methylene blue (MB).

Introduction

Industrial and agricultural processes produce large volumes of organic effluents which are toxic and non-biodegradable. A number of physical operations (*e.g.*, reverse osmosis, ion exchange, ultrafiltration, precipitation and adsorption, among others) are available for the removal of organic pollutants from contaminated waters, adsorption being, by far, the most versatile and widely used one.^{1,2} However, these technologies only offer the removal of the pollutant, meaning non-biodegradable compounds are ultimately transferred into a sludge which needs chemical treatments for its regeneration.^{3–5} This is why advanced oxidation technologies, such as semiconductor-mediated photocatalysis, are gaining popularity for the decontamination of wastewater, since they offer complete contaminant mineralization.⁶ Among the different semiconductors, titanium dioxide (TiO₂) has been the photocatalyst of choice, due to its strong oxidizing power, chemical and biological inertness, long term photostability and low cost.⁷ In particular, a commercial TiO₂ polycrystalline nanopowder, Degussa P25, which has a low space-charge recombination, made of anatase (80%) and rutile (20%) allotropic phases, has exhibited enhanced photocatalytic activity in wastewater treatment. The best performance was

obtained when the powders were used in well mixed suspensions, both in batch or continuous photoreactions; this way of utilization, however, presents the main drawback that a separation unit must be added to take the powder out of the reaction medium, thus increasing the complexity and cost of treatment.

Several strategies have been proposed to overcome these problems, the most successful being the use of TiO₂ nanoparticles anchored onto or embedded into preformed porous substrates (*i.e.* zeolites, clay minerals,^{8,9} activated carbons^{10,11} and silica¹²) and the use of porous titania based materials with hierarchical structures obtained through template synthesis.^{13–16} We, and others, have recently demonstrated the suitability of a cryogenic process (so called ice-segregation induced self-assembly, ISISA) for the preparation of inorganic, organic and hybrid macroporous monoliths and fibres, which, eventually, can be hierarchically organized.^{14,17–21} The ISISA is a bottom-up process that is based on the unidirectional immersion of a colloidal aqueous suspension into liquid nitrogen. The ice formation causes most solutes originally dispersed in the aqueous suspension to be segregated from the ice phase, giving rise to a macroporous structure, characterized by “fences” of matter enclosing ice. The scaffolds obtained after subsequent drying (by both thawing and freeze-drying) show a macroporosity that corresponds to the empty areas where ice crystals originally resided. Such highly open macro-channelled structures are highly suitable for performing catalytic reactions.^{14,18} It is important to outline that hierarchical monoliths exhibit a macro- and meso/micro-porous structure, the former allowing for easy mass transport while the latter provides large surface areas and hence, efficient catalytic activities. Moreover, the ability to use the sol–gel process allows the reinforcement of the nano-structured character of hierarchical materials and it might eventually allow control of the hydrophobicity of prepared materials through the use of organically modified ceramics (Ormocers), which have been demonstrated to improve the photocatalytic properties of silica/titania nanocomposites.¹²

^aInstituto de Ciencia de Materiales de Madrid, CSIC, Campus de Cantoblanco, 28049 Madrid, Spain. E-mail: mferrer@icmm.csic.es

^b“Schiavello-Grillone” Photocatalysis Group, Dipartimento di Ingegneria Chimica dei Processi e dei Materiali, Università degli Studi di Palermo, viale delle Scienze, 90128 Palermo, Italy. E-mail: augugliaro@dicpm.unipa.it

^cIstituto per lo Studio dei Materiali Nanostrutturati, CNR, via Ugo La Malfa 153, 90146 Palermo, Italy

^dKimya Bölümü, Fen Fakültesi, Anadolu Üniversitesi, Yunus Emre Kampüsü, 26470 Eskisehir, Turkey

† Electronic supplementary information (ESI) available: TEM images of aqueous suspensions of titania nanoparticles and sepiolite fibres as well as adsorption graphs of the pollutants over time. See DOI: 10.1039/b813864h

In this work we have used the ISISA process to prepare monolithic pieces exhibiting a microchannelled structure. The monoliths were composed of polycrystalline TiO_2 Degussa P25 nanoparticles (widely used in photocatalytic systems) adsorbed onto sepiolite fibres, and glued together using colloidal silica resulting from hydrolysis and condensation of an alkoxysilane precursor (*e.g.*, TEOS). Sepiolite, a hydrated magnesium silicate, with the ideal formula $\text{Si}_{12}\text{Mg}_8\text{O}_{30}(\text{OH})_4 \cdot 8\text{H}_2\text{O}$, is a non-swelling, lightweight, porous clay mineral with a large specific surface area. Its high surface area and porosity, as well as its needle-like morphology, account for its outstanding sorption capacity. The combination of such a different species into a single macroporous structure provides a multifunctional system capable of water decontamination by pollutant removal from aqueous media *via* adsorption on sepiolite, and subsequent elimination by UV irradiation *via* photocatalytic effect of TiO_2 nanoparticles. The combination of adsorption and photoreaction enhances the contaminant removal from a thermodynamic and kinetic point of view: in fact the occurrence of contaminant degradation on the solid improves not only its capacity of adsorption, but also the driving force for the contaminant transfer from the liquid to the solid phase. The performance of the resulting monolithic materials has been studied using two contaminants often present in wastewater such as *p*-nitrophenol (PNP) and methylene blue (MB). PNP is used in the production of pesticides and synthetic dyes. Owing to its significant solubility in water, it is often present in wastewater¹¹ and its photocatalytic degradation has been widely used as a model for wastewater treatment.^{22–24} MB is extensively used for dyeing cotton, wood and silk, and its photocatalytic degradation has also been widely studied.^{25,26} In particular, we have characterized the prepared materials by scanning and transmission electron microscopy and by equilibrium adsorption isotherms, along with photocatalytic reactivity runs to evaluate the decontamination capabilities of these materials.

Experimental

Materials

Tetraethyl orthosilicate (TEOS), polyoxyethylene ($n = 12$) nonylphenylether, (IGEPAL CO-720), methylene blue (MB) and *p*-nitrophenol (PNP) were purchased from Sigma-Aldrich Chemical Co. (Milwaukee, WI, USA) and were used without further purification. A natural mineral containing >95% of pure sepiolite from the Vallecas-Vicálvaro clay deposits (Madrid, Spain) and commercialized as Pangel S-9 (water suspension having 6 wt% in sepiolite) was provided by TOLSA. Polycrystalline titanium dioxide powder composed of an anatase-rutile mixture (with *ca.* 80 : 20 ratio, $50 \text{ m}^2 \text{ g}^{-1}$, PZC 6.1) and commercialized as Degussa P25 was provided by Degussa AG Company (Germany). Other chemicals were of analytical or spectroscopic reagent grade. Doubly distilled water ($R > 18 \text{ M}\Omega \text{ cm}$) was used. All other chemical compounds were used as received from Sigma-Aldrich.

Silica sol preparation. Silica sols were prepared using a reported protocol for biomolecule encapsulation.²⁷ Briefly, 4.0 mL TEOS, 1.25 mL H_2O and 36 μL HCl (0.62 M) were mixed under

vigorous stirring at 22 °C in a closed vessel. After 1 hour, 1 mL of the resulting sol was mixed with 1 mL of deionized water and underwent vacuum evaporation at 40 °C producing a weight loss of 0.62 g (this is approximately equal to the loss of ethanol which resulted from alkoxyde hydrolysis).

Silica–sepiolite and titania–silica–sepiolite hydrogel preparation. Silica–sepiolite hydrogels were prepared by the addition of 835 μL deionized water to 415 mg Pangel S-9 (6% w/v) water suspension (25 mg sepiolite). The resulting suspension (Fig. S1, ESI†) was vortexed to ensure homogeneity followed by the addition of 250 μL of the silica sol described above. Hydrogel formation occurred readily after mixing. Titania–silica–sepiolite hydrogels were prepared by the addition of 22.5 mg TiO_2 Degussa P25 nanopowder to 835 μL of deionized water. The suspension was sonicated (Vibra Cell, 500 W, 20 kHz, Sonic and Materials, Danbury, USA) for 30 min using cycles of irradiation and no-irradiation of 15 and 5 s, respectively, to ensure the disaggregation of eventually aggregated titania nanoparticles (Fig. S1, ESI†). The resulting titania suspension was added to 415 mg Pangel S-9 (6% w/v) suspension in water (25 mg sepiolite) and vortexed. Hydrogel formation also occurred readily after the addition of 250 μL of silica sol. In both cases, hydrogels were aged at room temperature for 4 h. The sepiolite and titania contents were 1.67% and 1.5%, respectively. The use of non-ionic surfactant (Igepal CO-720, 1.8% w/v) for the preparation of a titania suspension was also explored. In this case, the scaffolds needed either extensive washing with absolute ethanol for 24 h or calcination at 500 °C for surfactant removal prior to adsorption and photocatalytic experiments.

ISISA processing for scaffold preparation. Unless otherwise specified, every suspension (1 mL) was collected into insulin syringes and dipped at a constant rate of 5.9 mm min⁻¹ into a liquid nitrogen bath (-196 °C). The unidirectionally frozen samples were freeze-dried using a ThermoSavant Micromodulyo freeze-drier. The resulting monoliths kept both the shape and the size of the container where the suspensions were eventually collected prior to freezing (Fig. S2, ESI†).

Sample characterization. Sample morphologies were investigated by scanning and transmission electron microscopy (SEM and TEM). SEM and TEM were recorded using a Zeiss DSM-950 instrument and a 200 keV JEOL-2000, respectively. Gold metalized samples were prepared by using a Sputtering Balzers (SCD-004). Surface area measurements were performed on a FlowSorb 2300 from Micromeritics. Samples were thermally treated at 300 °C under an inert atmosphere for 30 min before measurements were taken.

Adsorption studies. A Varian-Cary 4000 spectrophotometer was used for the evaluation of the adsorption properties of the different scaffolds. The adsorption kinetics were studied in cuvettes containing monolithic scaffolds (20 mg) and 3 mL solutions of either PNP or MB at different concentrations. The supernatants were analyzed at given time intervals by absorption spectrophotometry at fixed wavelengths, *i.e.* 665 nm for MB and 318 nm for PNP (Fig. S3, ESI†). The equilibrium experiments were performed by soaking different amounts of monolithic

scaffolds in 5 mL of a solution containing a fixed contaminant amount (PNP or MB). After 24 h, the scaffolds were removed from the solution and the remaining dye was measured by absorption spectrophotometry. The adsorption isotherms were measured by taking fixed amounts of adsorbent scaffolds (40 mg), which were submerged in 5 mL of a dye solution at different concentrations and left to adsorb for 24 h at 20 °C. Afterwards, the scaffolds were removed from the solution and the remaining contaminant concentration was measured by absorption spectrophotometry. Experiments were conducted in triplicate. Averaged data was used for the representation of Langmuir and Freundlich isotherms (Fig. 4). The standard deviation was less than 5%.

The amount of adsorbed substrate per unit of adsorbent mass at equilibrium concentration, q_e (in mg g⁻¹) was calculated from the mass balance equation:

$$q_e = \frac{C_0 - C_e}{m/V} \quad (1)$$

where C_0 and C_e are the initial and equilibrium substrate concentrations (mg L⁻¹), V is the volume of the liquid phase (in L) and m is the mass of the adsorbent scaffold (in g). The Langmuir isotherm is given by the following equation:²⁸

$$q_e = \frac{MK_L C_e}{1 + K_L C_e} \quad (2)$$

where M is the maximum adsorption capacity (mg g⁻¹), and K_L is the equilibrium adsorption constant related to the adsorption energy (L mg⁻¹). The Freundlich isotherm²⁹ is given by the following equation:

$$q_e = K_F(C_e)^n \quad (3)$$

where K_F and n are the Freundlich constants related to the adsorption capacity and intensity, respectively. The equilibrium constants for these models were derived using linear regression analysis.

Photocatalytic reactivity. Photocatalytic runs for the oxidation of the aromatic compounds were performed in duplicate in both the liquid–solid and gas–solid regime. The active photocatalyst, P25, either free or inside the scaffolds, was used (0.28 g L⁻¹) in powdered form when performing liquid–solid runs. For PNP, the experiments were carried out at pH 4, when the solution is transparent and does not undergo homogeneous oxidation, and at *ca.* pH 7 for MB. The liquid–solid experiments were performed in a batch photoreactor of cylindrical shape, containing 0.5 L of aqueous suspension, continuously bubbling with pure O₂. A 125 W medium-pressure Hg lamp (Helios Italquartz, Italy) was axially immersed within the photoreactor. The lamp was cooled by water circulating through a Pyrex thimble. The temperature of the suspension was about 25 °C. The radiation energy impinging on the suspension had an average value of 10 mW cm⁻² (measured by using a radiometer UVX Digital at $\lambda = 360$ nm). The initial concentration of the substrates in the liquid–solid experiments was *ca.* 150 µM. This amount was either pre-adsorbed onto the scaffold surface or dissolved in water followed by the addition of the bare scaffolds. During the photocatalytic runs, samples for analyses were withdrawn at fixed intervals of

time and the catalyst was immediately separated from the aqueous solution by filtering through a 0.45 µm hydrophilic membrane (HA, Millipore). The species concentration in the liquid phase was monitored through absorption spectrophotometry for both PNP and MB. Averaged data was used for the representation of photocatalytic oxidations (Fig. 5 and 6). The standard deviation was also less than 5%. Further gas–solid experiments were performed by irradiating dry SS-P25 monolithic scaffolds using a 400 W medium-pressure Hg lamp (Fig. S4, ESI†). As in previous experiments, MB was adsorbed on the SS-P25 monolithic scaffolds from an aqueous MB solution (150 µM).

Results and discussion

The synthetic approach used for the integration of every component (silica, sepiolite and TiO₂ P25 nanoparticles) into the resulting hierarchical structure was as follows. We first prepared two separate aqueous suspensions of well dispersed sepiolite and TiO₂ P25 nanoparticles, respectively (Fig. S1, ESI†). The use of surfactants (*e.g.*, non-ionic Igepal CO-720) for the preparation of TiO₂ P25 nanoparticle suspensions also resulted in a good dispersion of the nanoparticles, but the use of surfactants was finally discarded given that further sample treatments (*e.g.*, either ethanol washing or thermal treatment) were required to eliminate the surfactant before submitting the scaffolds to contaminant adsorption. Otherwise, the adsorption capability of the resulting materials was strongly reduced. The resulting water suspensions of sepiolite and P25 nanoparticles were mixed so that P25 nanoparticles were adsorbed onto the sepiolite fibres. The adsorption of TiO₂ P25 nanoparticles onto the sepiolite fibres helped to minimize the eventual formation of TiO₂ P25 nanoparticle aggregates (Fig. 1). The water suspension, composed of sepiolite and P25 nanoparticles, was added to the aqueous silica sol, promoting silica condensation and, thus, the formation of the inorganic hydrogels. The aqueous silica sol was prepared through a reported protocol that ensured the elimination of the

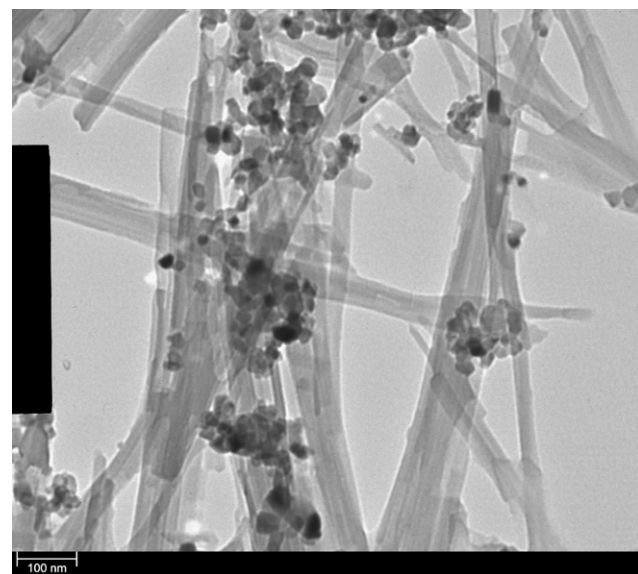


Fig. 1 TEM micrographs of TiO₂ Degussa P25 adsorbed on sepiolite fibres. Bar is 100 nm.

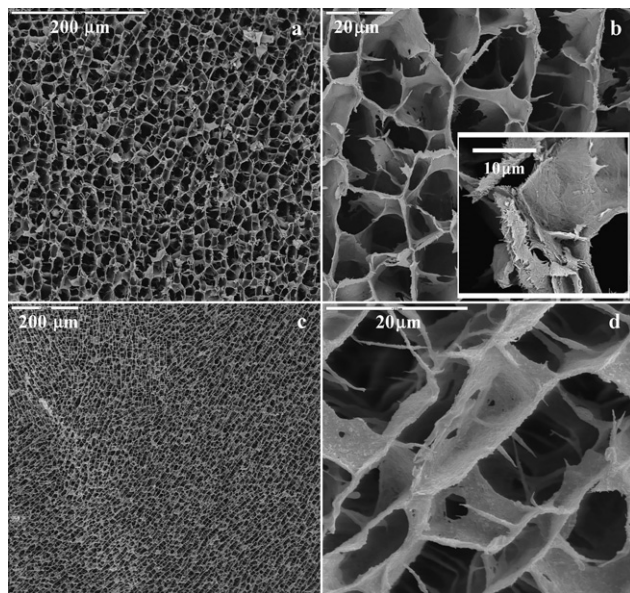


Fig. 2 SEM micrographs of cross-sectioned SS (a and b) and SS–P25 scaffolds (c and d). Bars are 200 μm in (a) and (c), and 20 μm in (b) and (d). Inset in (b) shows the detail of SS structures (bar 10 μm).

alcohol released during the sol–gel process.²⁷ Alcohol removal was crucial in obtaining a hydrogel suitable for application in the ISISA process. Otherwise, formation of ice crystals could be altered or even partially impeded. The overall weight percentage of silica, sepiolite and TiO_2 P25 nanoparticles forming the hydrogels was adjusted to 5.6 for silica–sepiolite–P25 (SS–P25) scaffolds, within a suitable range for the formation of highly open interconnected macroporous structures (*e.g.*, 4–10 wt%).¹⁹ The TiO_2 weight percent ratio on the scaffolds was *ca.* 27 wt%, given the excellent photocatalytic results recently reported for TiO_2 –Ca-montmorillonite composites within this range of concentrations (*e.g.* TiO_2 25 wt%).¹⁰ Silica–sepiolite (SS) scaffolds were also prepared as controls (positive for adsorption and negative for photocatalysis), having 4.1 wt% overall weight percentage of silica and sepiolite in the hydrogel (see Experimental). Hydrogels were aged for 4 h to enhance the robustness of the scaffolds resulting after the application of the ISISA process. The application of the ISISA process to such aged hydrogels resulted in the formation of hierarchically structured monoliths composed of silica, sepiolite and P25 nanoparticles homogeneously distributed throughout the whole macroporous structure (Fig. 2). Interestingly, SEM micrographs revealed the microchannelled structure of the SS and SS–P25 scaffolds that occurred as a consequence of the unidirectional freezing that characterizes the ISISA process. The highly open microchanneled structure of the monolithic pieces ensured accessibility of small molecules to their inner structure. A close inspection of the SEM micrographs enabled the observation of individual sepiolite fibres dispersed within the silica matrix (in both SS and SS–P25 scaffolds) and of small nanoaggregates (ascribed to P25 nanoparticles) onto the sepiolite fibres (only in SS–P25 scaffolds), in good concordance with previous TEM micrographs. Thus, the walls that support the three dimensional architectures were mostly composed of self-assembled sepiolite fibres and colloidal silica formed by hydrolysis and condensation of TEOS. The

excellent compatibility among both components (as mentioned above, sepiolite was homogeneously distributed within the silica matrix) enabled good mechanical stability of the obtained scaffolds.

The scaffolds adsorption properties were evaluated with water solutions ($\text{pH} \approx 6$) containing pollutant organic species of different natures; *e.g.*, the neutral PNP and the cationic MB. Anionic pollutants were not tested in this work given that the isoelectric point of the scaffold components, *i.e.*, 2.5 for silica,³⁰ 2.2 for sepiolite³¹ and 6.0 for P25,³² would lead to their unfavourable adsorption at the working pH. The equilibrium experiments were performed on scaffolds immersed in dye solutions for 24 h to ensure full dye adsorption (see the adsorption kinetics for MB and PNP in Fig. S3, ESI†). The adsorption efficiency of the scaffolds is depicted in Fig. 3, showing the amount of organic pollutant remaining in solution after scaffold saturation as a function of the quantity of adsorbent. The plot of the cationic dye MB presented a low equilibrium concentration in solution at low adsorbent doses, therefore indicating that MB was readily absorbed by the negatively charged scaffolds due to favourable electrostatic attractions. Adsorption experiments on SS scaffolds (without TiO_2 P25 nanoparticles) exhibited a similar trend, but close inspection of the plot revealed some scaffold capability enhancement for MB adsorption, most likely due to the overall decrease of the nanocomposite PZC³¹ and the increase of the surface area (*i.e.*, 365 m^2g^{-1} for SS versus 290 m^2g^{-1} for SS–P25). Data obtained from adsorption isotherms were fitted to Langmuir and Freundlich^{33,12} adsorption models (Fig. 4). The obtained fitting parameters together with the correlation coefficients (R^2) are listed in Table 1. Thus, the Freundlich model provided the best correlation data with an exponent <1 , indicative of favoured adsorption.³⁴ The good fit of data to this model also denoted that the heterogeneous site adsorption energy for MB suggested a multilayer adsorption process that may result from dye aggregation on the sepiolite surface.^{33a,35} The adsorption equilibrium constant K_F , that represents the adsorption capacity of the scaffold, corroborated the higher adsorption capability of SS versus SS–P25 for MB. Meanwhile, the overall adsorption of the neutral PNP on both SS–P25 and SS scaffolds was in the range reported for phenol adsorbed on raw or

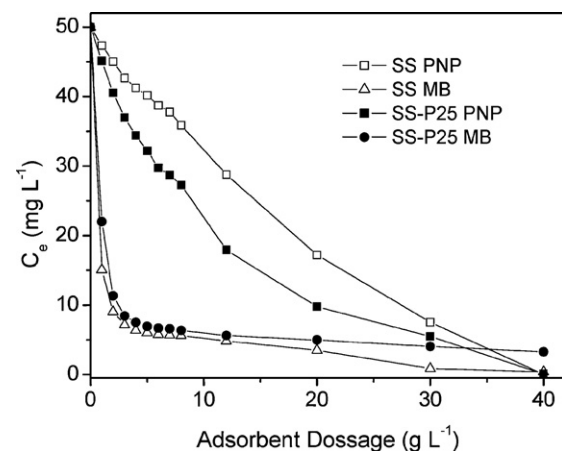


Fig. 3 Plot of contaminant equilibrium concentration remaining in solution after adsorption for 24 h on scaffolds versus adsorbent scaffold dosage.

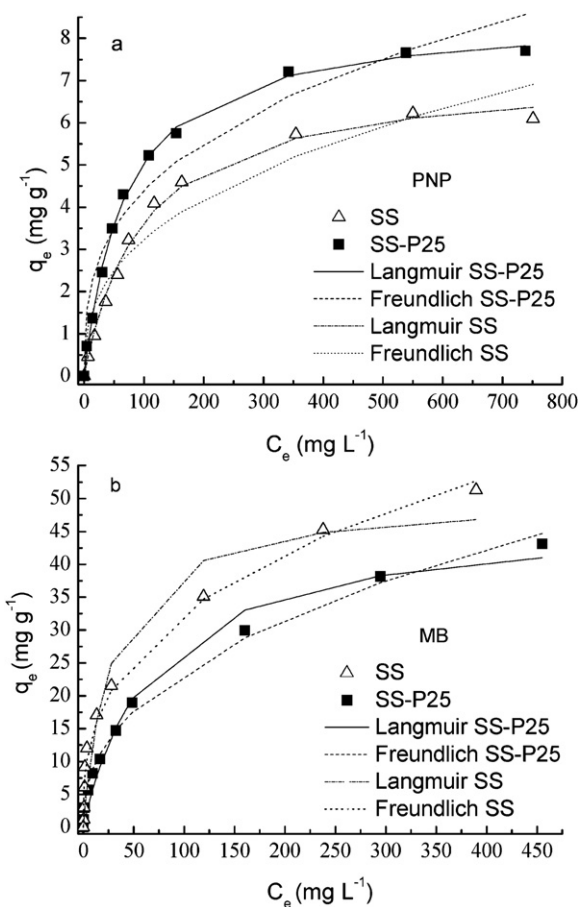


Fig. 4 Langmuir and Freundlich adsorption isotherms of PNP (a) and MB (b) on SS and SS-P25 scaffolds.

Table 1 Langmuir and Freundlich isotherm adsorption constants for MB and PNP on the prepared scaffolds

Contaminant	Scaffold	Langmuir's model		Freundlich's model			
		K_L (L mg ⁻¹)	M (mg g ⁻¹)	R^2	K_F^a	n	R^2
MB	SS	0.0355	50.2	0.950	6.44	0.352	0.989
	SS-P25	0.0146	47.2	0.985	3.40	0.421	0.995
PNP	SS	0.0102	7.19	0.995	0.58	0.375	0.934
	SS-P25	0.0145	8.55	0.998	0.95	0.333	0.948

^a The dimension of K_F depends on n . The reported values have been obtained by expressing q_e in mg g⁻¹ and C_e in mg L⁻¹.

thermally activated sepiolite,³⁶ albeit moderately compared to those mentioned above for MB. Note that organic (rather than inorganic) adsorbent materials (*e.g.*, activated carbons,³⁷ ureasil gels³⁸ or organically modified clay minerals,³⁹ among others) are recommended in those cases (*e.g.*, phenol and nitrophenols) where adsorption is not governed by electrostatic interactions.

Photocatalytic measurements were performed on SS-P25 scaffolds containing contaminants by exposing the samples to UV radiation. Samples were powdered and suspended in water for a total solid content of 0.1 wt%. Having in mind that the

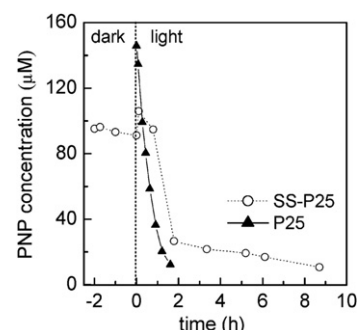


Fig. 5 Plot representing PNP concentration *versus* irradiation time in solutions containing pristine P25 and powdered SS-P25 scaffolds.

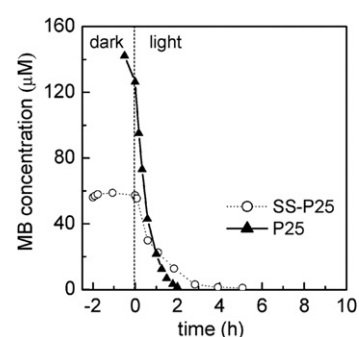


Fig. 6 Plot representing MB concentration *versus* irradiation time in solutions containing pristine P25 or powdered SS-P25 scaffolds.

scaffolds were composed of sol–gel silica (43%), sepiolite (30%) and P25 nanoparticles (27%), the P25 content in the water suspension was *ca.* 0.135 g. For comparison, PNP and MB adsorbed on SS scaffolds were studied as negative controls, while PNP and MB dissolved in a Degussa P25 water suspension were studied as positive controls. In this later case, the amount of P25 catalyst was adjusted to 0.14 g (0.028 wt%) to keep constant the amount of photoactive species in the range to those in SS-P25 scaffolds. Fig. 5 shows that the PNP degradation after irradiation for 90 min reached values of 92% and 82% for pure P25 nanoparticles and SS-P25 scaffolds, respectively, while it was negligible for SS scaffolds (data not shown). Fig. 6 shows that MB degradation after *ca.* 2 h of irradiation reached values of 94% and 86% for pure P25 nanoparticles and SS-P25 scaffolds, respectively, and was negligible when using SS scaffolds. In both cases (PNP and MB), the degradation percentage found for SS-P25 scaffolds was quite comparable (only 10% lower) to that of pure P25 nanoparticles, even though the occurrence of TiO₂ P25 nanoparticle adsorption on the scaffold may result in partial inaccessibility to the active surface. It is also worth noting that the SS-P25 suspension is optically less transparent (it is more concentrated than that of pure P25 nanoparticles: 0.1 wt% *versus* 0.028 wt%) so irradiation is less effective due to light scattering losses. It should be mentioned that, since scaffolds are prepared through a lyophilisation process, some wetting treatment prior to irradiation was required for efficient degradation rates. Finally, we exposed a monolithic SS-P25 scaffold to light irradiation which, after MB adsorption, was left to dry at room temperature. The decolouration observed in Fig. S4 (ESI†) helped to illustrate

the photocatalytic efficiency of SS-P25 scaffolds even in non favoured (*e.g.* gas–solid) conditions.

Conclusions

In this work, we have prepared multifunctional materials that consist of a macroporous structure supported by silica–sepiolite–titania nanocomposites which combine high adsorption capability and self-regenerative (by UV irradiation) properties. Such a high adsorption capability has to be ascribed not only to the presence of sepiolite, but also to the hierarchical macro- and mesoporous structure allowing sepiolite accessibility. The adsorption equilibrium experiments revealed that sepiolite fibres kept their sorption ability (higher for cationic MB than for PNP) regardless of their integration within the nano-structured walls supporting the hierarchical structure. Meanwhile, the presence of TiO₂ P25 nanoparticles within the hierarchical structure promoted efficient (in a similar range to that found for pristine P25 nanoparticles in water suspensions) elimination of the adsorbed pollutant by typical photooxidation processes. Actually, the decolouration obtained by exposition of the coloured hierarchical structure to direct UV irradiation was remarkable even in dry conditions. The efficiency of these hierarchical structures, in terms of both species adsorption and UV induced decolouration, opens the path to the use of these materials as membranes in flow operation mode, similarly to monolithic columns used in chromatography and other separation applications. Moreover, the use of additives (surfactants), functionalized sepiolite and/or silica precursors (*e.g.*, organically modified) would open the possibility to prepare hierarchical structures with controlled surface areas (within the mesopore range) and balanced hydrophobic/hydrophilic character. The versatility of the resulting materials would contribute in an overall enhancement of both adsorption and photocatalytic performance.

Acknowledgements

This work was supported by MEC (MAT2006-02394 Project), CM (S-0505/PPQ-0316 Project) and CSIC (200760I009 and 200660F01 Projects). M. N.-S. acknowledges TPA and CSIC for an I3P postdoctoral research contract. M. C. G. acknowledges MICINN for an R&C research contract.

References

- J. Wu, C. Liu, K. H. Chu and S. Y., *J. Membr. Sci.*, 2008, **309**, 239–245.
- V. K. Gupta, S. I. Ali and V. K. Saini, *Ind. Eng. Chem. Res.*, 2004, **43**, 1740–1747.
- S. K. Kansal, M. Singh and D. J. Sud, *J. Hazard. Mater.*, 2007, **141**, 581–590.
- W. S. Kuo and P. H. Ho, *Chemosphere*, 2001, **45**, 77–83.
- I. Ilisz, A. Dombi, K. Mogyorósi, A. Farkas and I. Dékány, *Appl. Cat. B*, 2002, **39**, 247–256.
- (a) *Heterogeneous Photocatalysis*, ed. M. Anpo, H. Yamashita, and M. Schiavello, Wiley, Chichester, 1997, p. 133; (b) *Photocatalytic Purification and Treatment of Water and Air*, ed. D. F. Ollis, and H. Al-Ekabi, Elsevier, Amsterdam, 1993.
- M. R. Hoffman, S. T. Martin, W. Y. Choi and D. W. Bahnemann, *Chem. Rev.*, 1995, **95**, 735–758.
- P. Aranda, R. Kun, M. A. Martín -Luengo, S. Letaïef, I. Dékany and E. Ruiz-Hitzky, *Chem. Mater.*, 2008, **20**, 84–91.
- J. Ménesi, L. Körösi, E. Bazsó, V. Zöllmer, A. Richardt and I. Dékány, *Chemosphere*, 2008, **70**, 538–542.
- Q. Wang, D. Yang, D. Chen, Y. Wang and Z. Jiang, *J. Nanopart. Res.*, 2007, **9**, 1087–1096.
- K. Nagaveni, G. Silvalingam, M. S. Hegde and G. Madras, *Environ. Sci. Technol.*, 2004, **38**, 1600–1604.
- G. Dagan, S. Sampath and O. Lev, *Chem. Mater.*, 1995, **7**, 446–453.
- J. H. Schattka, D. G. Shchukin, J. Jia, M. Antonietti and R. A. Caruso, *Chem. Mater.*, 2002, **14**, 5103–5108.
- S. R. Mukai, H. Nishihara, S. Shichi and H. Tamon, *Chem. Mater.*, 2004, **16**, 4987–4991.
- D. G. Shchukin, J. H. Schattka, M. Antonietti and R. A. Caruso, *J. Phys. Chem.*, 2003, **107**, 952–957.
- H. Choi, E. Stathatos and D. Dionysiou, *Appl. Cat. C*, 2006, **63**, 60–67.
- M. L. Ferrer, R. Esquembre, I. Ortega, C. R. Mateo and F. del Monte, *Chem. Mater.*, 2006, **18**, 554–559.
- M. C. Gutierrez, M. L. Ferrer and F. del Monte, *Adv. Mater.*, 2006, **18**, 1137–1140.
- (a) M. C. Gutierrez, M. L. Ferrer and F. del Monte, *Chem. Mater.*, 2008, **20**, 634–648; (b) M. C. Gutierrez, Z. Y. Garcia-Carvajal, M. Jobbagy, F. Rubio, M. L. Ferrer and F. del Monte, *Adv. Funct. Mater.*, 2007, **17**, 3505–3513; (c) M. C. Gutierrez, M. J. Hortigüela, M. Amarilla, R. Jiménez, M. L. Ferrer and F. Del Monte, *J. Phys. Chem. C*, 2007, **111**, 5557–5560.
- (a) H. Nishihara, S. R. Mukai, D. Yamashita and H. Tamon, *Chem. Mater.*, 2005, **17**, 683; (b) S. Deville, E. Saiz, R. K. Nalla and A. P. Tomsia, *Science*, 2006, **311**, 515–518.
- (a) H. Zhang, I. Hussain, M. Brust, M. F. Butler, S. P. Rannard and A. I. Cooper, *Nat. Mater.*, 2005, **4**, 787; (b) Q. Shi, Z. An, C. Tsung, H. Liang, N. Zheng, C. J. Hawker and G. D. Stucky, *Adv. Mater.*, 2007, **9**, 4539–4543.
- V. Augugliaro, M. J. López, L. Palmisano and J. Soria, *Appl. Catal. A*, 1993, **101**, 7–13.
- D. Chen and A. Ray, *Water Res.*, 1998, **32**, 3223–3234.
- W. Y. Ahn, S. A. Sheeley, T. Rajh and D. M. Cropek, *Appl. Catal. B*, 2007, **74**, 103–110.
- (a) E. A. El-Sharkawy, A. Y. Soliman and K. M. Al-Mer, *J. Colloid Interface Sci.*, 2007, **302**, 498–508; (b) H. Lachheb, E. Puzenat, A. Houas, M. Ksibi, E. Elaloui, C. Guillard and J.-M. Herrmann, *Appl. Catal.*, 2002, **39**, 75–90.
- W. Tsai, H. Hsu, T. Su, K. Lin and C. Lin, *J. Hazard. Mater.*, 2008, **154**, 73.
- M. L. Ferrer, F. del Monte and D. Levy, *Chem. Mater.*, 2002, **14**, 3619–3621.
- I. Langmuir, *J. Am. Chem. Soc.*, 1918, **40**, 1361.
- H. Freundlich, *Colloid and Capillary Chemistry*, Methuen, London, 1926.
- G. Ramos, F. del Monte, M. Zayat, M. L. Ferrer and D. Levy, *J. Sol-Gel Sci. Technol.*, 2003, **26**, 869–872.
- C. Knapp, F. J. Gil-Llambias, M. Gulppi-Cabra, P. Avila and J. Blanco, *J. Mater. Chem.*, 1997, **7**, 1641–1645.
- F. Y. Oliva, L. B. Avalle, O. R. Cámara and C. P. De Pauli, *J. Colloid Interface Sci.*, 2003, **261**, 299–311.
- (a) Y. El Mouzdahir, A. Elmchaouri, R. Mahboub, A. Gil and S. A. Korili, *J. Chem. Eng. Data*, 2007, **52**, 1621; (b) E. A. El-Sharkawy, A. Y. Soliman and K. M. Al-Amer, *J. Colloid Interface Sci.*, 2007, **310**, 498–508.
- R. Dhodapkar, N. N. Rao, S. P. Pande, T. Nandy and S. Devotta, *React. Funct. Polym.*, 2007, **67**, 540–548.
- A. J. Aznar, B. Casal, E. Ruiz-Hitzky, I. López -Arbeloa, F. López Arbeloa, J. Santaren and A. Alvarez, *Clay Min.*, 1992, **27**, 101–108.
- M. Ugurlu, A. Gurses, M. Yalcin and C. Dogar, *Adsorption*, 2005, **11**, 87–91.
- A. Kumar, S. Kumar, S. Kumar and D. V. Gupta, *J. Hazard. Mater.*, 2007, **147**, 155–166.
- V. Bekiari and P. Lianos, *Chem. Mater.*, 2006, **18**, 4142–4146.
- D. I. Song and W. S. Shin, *Environ. Sci. Technol.*, 2005, **39**, 1138–1143.